Journal of Physical Science
Vol. 37(2), 51–71, 2026

First-Principles Study of Fe_2O_3-Doped Graphene: Structural, Electronic, Magnetic and Optical Insights

Hayder M. Hadi

Department of Medical Physics - College of Science - University of Al-Qadisiyah
Al-Diwaniya 58001, Iraq

*Corresponding author: hayder.mohammed@qu.edu.iq

Published online: 28 August 2026

To cite this article: Hadi, H. M. (2026). First-principles study of Fe_2O_3-goped graphene: Structural, electronic, magnetic and optical insights. *J. Phys. Sci.*, 37(2), 51–72. https://doi.org/10.21315/jps2026.37.2.4

To link this article: https://doi.org/10.21315/jps2026.37.2.4

ABSTRACT: This study presents a comprehensive theoretical investigation into how iron (III) oxide (Fe_2O_3) doping alters the structural, electronic, optical, magnetic and thermodynamic properties of graphene. A finite-size C52 graphene cluster was used to simulate localised doping effects using Density Functional Theory (DFT) and Time-Dependent DFT (TD-DFT). The introduction of Fe_2O_3 significantly reduced the bandgap to ~1.6 eV and introduced mid-gap states, indicating enhanced semiconducting behaviour and reactivity, as confirmed by highest occupied molecular orbital and the lowest unoccupied molecular orbital (HOMO–LUMO) gap and density of states (DOS) analyses. Optical simulations revealed increased absorbance in the visible spectrum, with characteristic peaks at 310 nm and 395 nm linked to Fe-graphene hybrid orbitals. Magnetic property analysis revealed increased anisotropy and shielding near Fe and O atoms, indicating the formation of localised magnetic moments. Structurally, Fe–C and Fe–O bonds formed stably, with minimal lattice distortion. Vibrational and thermodynamic analyses confirmed increased thermal stability and lower formation enthalpy. The novelty of this work lies in employing a finite-cluster DFT/TD-DFT model that captures localised Fe–O–C interactions and anisotropic magnetic behaviour, which are often overlooked in periodic systems. This integrated approach simultaneously explains the structural, electronic, and optical coupling mechanisms in Fe_2O_3-doped graphene, providing molecular-level insights consistent with experimental observations but previously unquantified theoretically. These findings highlight the potential of Fe_2O_3-doped graphene in optoelectronic devices, photocatalysis, spintronics and energy-related applications.

Keywords: DFT, graphene, doping, iron oxide, Fe_2O_3.

1. INTRODUCTION

Graphene is a two-dimensional carbon material composed of sp^2-hybridised atoms arranged in a hexagonal lattice, well known for its high electrical conductivity, mechanical robustness and optical transparency. These properties have positioned graphene as a promising platform for applications in nanoelectronics, sensing and energy-related devices. Beyond extended periodic sheets, finite graphene clusters have attracted increasing theoretical interest, as they enable the explicit treatment of edge effects, localised states and site-specific interactions that are often underestimated in periodic models.[1–3] In addition, graphene exhibits a nearly constant visible-light absorption of approximately 2.3%, which allows its integration into transparent and optoelectronic architectures without significant optical losses.[2,4–6]

Despite these advantages, pristine graphene intrinsically lacks a bandgap and shows limited light–matter interaction, which restricts its direct use in semiconductor and optoelectronic technologies.[7–10] To overcome this limitation, chemical functionalisation and atomic or molecular doping have been widely explored as effective strategies for tailoring graphene's electronic and optical properties.[11,12] In particular, transition-metal oxides have emerged as attractive modifiers due to their ability to introduce localised electronic states, enhance optical absorption and induce magnetic behaviour. Among these oxides, iron (III) oxide (Fe_2O_3) is especially appealing because of its semiconducting character, strong magnetic anisotropy, chemical stability and broad absorption across the visible spectrum. When coupled with graphene, Fe_2O_3 has been shown to generate mid-gap states, modulate the band structure and promote efficient charge-transfer at the interface.[13–21]

Previous experimental and theoretical studies have demonstrated that Fe_2O_3–graphene composites can significantly influence charge redistribution, thermal stability and photocatalytic activity when compared with other oxide-modified systems such as titanium dioxide (TiO_2)–graphene or zinc oxide (ZnO)–graphene hybrids.[22–28] While TiO_2 and ZnO are effective photocatalysts under ultraviolet illumination, their weak magnetic response and limited visible-light absorption constrain their multifunctional performance. In contrast, Fe_2O_3 offers a balanced combination of bandgap tunability, optical responsiveness, and magnetic functionality, making it a promising dopant for advanced graphene-based nanostructures.[29–32]

However, despite the growing number of experimental and theoretical studies on Fe_2O_3–graphene composites, a detailed molecular-level understanding of how Fe_2O_3 incorporation simultaneously affects the electronic structure, optical response and magnetic anisotropy of graphene remains incomplete.

A critical limitation of many existing studies is that they either focus on experimental synthesis without detailed electronic-level interpretation or rely on periodic Density Functional Theory (DFT) models that tend to average out localised interfacial effects. Consequently, the microscopic mechanisms governing Fe_2O_3–graphene coupling—particularly the role of Fe–carbon (C) and Fe–O bonding in bandgap opening, mid-gap formation, magnetic anisotropy and optical excitations—remain insufficiently understood. Recent literature published after 2024 has emphasised the importance of combining structural and optical analyses to uncover such localised interactions in oxide-modified low-dimensional materials, yet comparable molecular-level insight for Fe_2O_3–graphene systems is still scarce.

In this context, the present study addresses this research gap by employing a finite-cluster first-principles framework based on DFT and time-dependent DFT (TD-DFT). By explicitly modelling a Fe_2O_3-decorated graphene cluster, this work systematically elucidates how molecular-scale Fe_2O_3 incorporation alters the structural integrity, electronic structure, magnetic behaviour and optical response of graphene. The results provide a unified interpretation of orbital hybridisation, charge redistribution and thermodynamic stability, offering new insight into the multifunctional potential of Fe_2O_3–graphene systems for applications in optoelectronics, photocatalysis and spintronics.

2. COMPUTATIONAL METHODOLOGY

All quantum chemical calculations were carried out using Gaussian 09.[32] Geometry optimisations and electronic structure analyses employed DFT with the Becke, three-parameter, Lee–Yang–Parr (B3LYP) hybrid functional for both ground and excited states. The 6-31G+(d,p) basis set was applied to carbon atoms, while Los Alamos National Laboratory 2 Double-Zeta (LanL2DZ) effective core potentials described Fe and O, ensuring reliable treatment of transition-metal interactions.

The model consisted of a finite graphene cluster (C_{52}). Pristine C_{52} and isolated Fe_2O_3 were optimised separately, after which Fe_2O_3 was placed on the graphene surface and the combined system fully optimised to obtain the most stable configuration.

The strength of interaction between graphene and Fe_2O_3 was evaluated via the binding energy, defined as:

$$E_{bind} = \left(Egraphene + E_{Fe_2O_3} \right) - Egraphene + \quad (1)$$

Where,

E_{bind}: Binding energy, which represents the strength of the interaction between graphene and Fe_2O_3.

$E_{graphene}$: Total energy of Pristine graphene.

$E_{Fe_2O_3}$: Total energy of Fe_2O_3.

$E_{graphene+Fe_2O_3}$: Total energy of the system after doping graphene with Fe_2O_3.

The Basis Set Superposition Error (BSSE) correction was not applied, which may slightly overestimate binding energies; however, the chosen level of theory remains reliable for qualitative and comparative analysis.

Optical properties were examined using TD-DFT (B3LYP/LANL2DZ), identifying electronic excitations relevant to the Ultraviolet–Visible (UV–Vis) spectrum. Natural bond orbital (NBO) analysis evaluated charge redistribution, while bond length variations revealed structural distortions affecting stability and reactivity.

Electronic properties were further probed by density of states (DOS) and frontier molecular orbitals (FMO) highest occupied molecular orbital–lowest unoccupied molecular orbital (HOMO–LUMO) analysis to quantify bandgap changes and assess semiconducting behaviour. Specific Fe_2O_3-induced transitions were correlated with enhanced optoelectronic response.

All simulations assumed finite molecular conditions, without periodic boundary sampling and used a closed-shell singlet configuration unless otherwise stated.

3. RESULTS AND DISCUSSION

3.1 Electronic Properties: HOMO–LUMO Distribution and Energy Gap

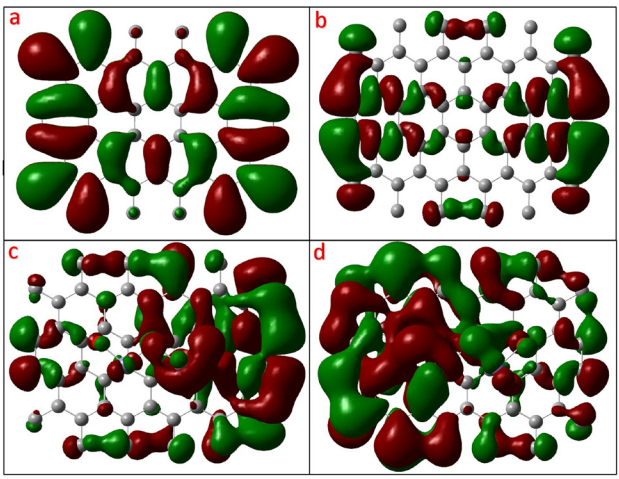

Figure 1: Molecular orbital iso surface plots of the HOMO and LUMO for both pristine and Fe_2O_3-doped graphene. (a) HOMO of pristine graphene; (b) LUMO of pristine graphene; (c) HOMO of Fe_2O_3-doped graphene; (d) LUMO of Fe_2O_3-doped graphene. The red and green regions represent opposite phases of the orbital wavefunctions.

Figure 1 shows the HOMO–LUMO distribution in pristine and Fe_2O_3-decorated graphene. In pristine graphene (Figures 1[a] and 1[b]), both orbitals are symmetrically delocalised, consistent with extended π-conjugation and a near-zero bandgap.

After Fe_2O_3 doping (Figures 1[c] and 1[d]), the HOMO localises on Fe and O atoms, while the LUMO becomes irregular with higher density near the dopant. This asymmetry indicates mid-gap states and localised transitions absent in the pristine system. The HOMO–LUMO gap increases to ~1.6 eV, exceeding the 1.1 eV–1.3 eV range reported for Fe-doped graphene, reflecting stronger orbital overlap and charge localisation.[33,34] Spatial separation between donor-like HOMO (near Fe_2O_3) and acceptor-like LUMO (across the lattice) enhances charge-transfer and UV–visible absorption.

The observed widening of the bandgap arises from orbital hybridisation between Fe 3d and C 2p states, which perturbs the π-electron cloud and induces partial charge-transfer from graphene to Fe_2O_3. This interaction breaks the electronic symmetry of the pristine sheet, leading to the formation of localised defect-like mid-gap states near

the Fermi level. These states act as controllable channels for carrier excitation, bridging the valence and conduction manifolds. The resulting electronic polarisation produces direction-dependent conductivity—an effect not previously reported for Fe_2O_3–graphene clusters of comparable size—highlighting the novelty of this mechanism within finite-model DFT studies.

3.2 Density of States

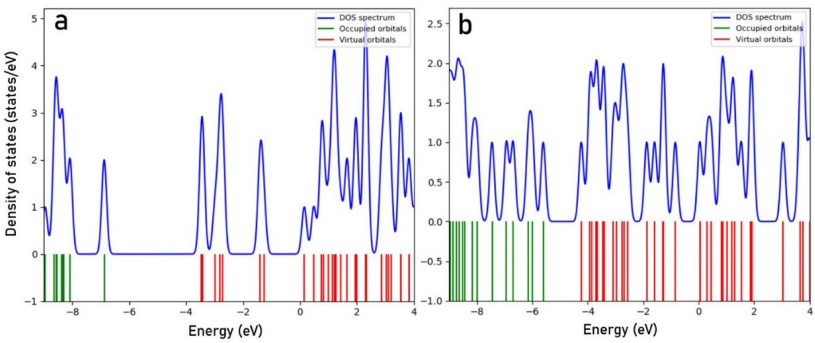

Figure 2: DOS plots for (a) pristine and (b) Fe_2O_3-doped graphene. Doping introduces mid-gap states near the Fermi level, enhancing electronic activity. Green and red lines represent occupied and virtual orbitals, respectively.

Figure 2 shows the DOS for pristine and Fe_2O_3-decorated graphene. In pristine graphene (see Figure 2[a]), occupied and unoccupied states are well separated, with a low density near the Fermi level, consistent with its delocalised π-system and semi-metallic nature.

After Fe_2O_3 doping (see Figure 2[b]), new states emerge near the Fermi level due to Fe 3d–π hybridisation, narrowing the bandgap and enhancing electron delocalisation. This increases transition probabilities, conductivity, and optical response. The broadened DOS and sharp peaks near the Fermi level indicate localised Fe–O–C activity, potentially serving as charge-trapping centres or catalytic sites.

The appearance of these narrow Fe-derived peaks is a clear manifestation of mid-gap state formation. The hybrid Fe 3d orbitals overlap with graphene's π-band, introducing localised donor and acceptor levels within the forbidden region. Such hybridised orbitals enable sub-band transitions and contribute to enhanced electrical conductivity under photoexcitation. Moreover, the coexistence of localised and delocalised states demonstrates a dual-character transport pathway, confirming that Fe_2O_3 doping transforms graphene from a purely semi-metallic to a tunable semiconducting system. This detailed DOS behaviour explains the physical mechanism behind the bandgap

modulation identified in the HOMO–LUMO analysis and reinforces the novelty of Fe_2O_3–induced electronic reconstruction.

Overall, DOS analysis demonstrates that Fe_2O_3 functionalisation boosts optoelectronic performance, with higher state density and mid-gap states supporting applications in photodetectors, solar cells and nanodevices.

3.3 Thermodynamic Energies of Fe_2O_3–Decorated Graphene

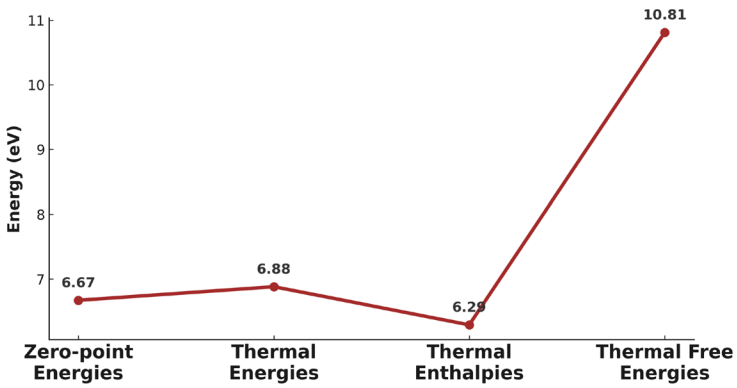

Figure 3: Thermodynamic energy components of Fe_2O_3-doped graphene obtained from DFT calculations, including zero-point energy, thermal energy, enthalpy and Gibbs free energy.

Figure 3 presents the thermodynamic energies of Fe_2O_3-functionalised graphene, including zero-point, thermal, enthalpy and free energy. The zero-point energy (6.67 eV) indicates a stable vibrational ground state, while thermal energy slightly increases to 6.88 eV. In contrast, enthalpy decreases to 6.29 eV, confirming favourable dopant–substrate interactions and enhanced stability. Free energy rises sharply to 10.81 eV, suggesting high energy availability for electron transfer and thermal excitation, relevant to catalysis, energy conversion and gas sensing.[35,36] Together, reduced enthalpy and elevated free energy define a thermodynamically favourable profile, with strong Fe_2O_3–graphene binding ensuring stability and functionality. In summary, Fe_2O_3 decoration stabilises the structure while enhancing energy responsiveness, supporting applications in optoelectronics, sensing and energy harvesting.[36,37]

The optical absorption spectrum of Fe_2O_3-decorated graphene further confirms these energetic trends. Two dominant absorption peaks are observed at approximately 310 nm and 395 nm, corresponding respectively to $\pi \rightarrow \pi$ transitions within the graphene lattice and charge-transfer transitions involving Fe 3d $\rightarrow$ C 2p hybrid orbitals. The first peak (310 nm) indicates excitation within the intrinsic conjugated network,

whereas the broader feature around 395 nm originates from Fe–O–C interfacial hybridisation, where Fe 3d states couple with graphene's π-electrons to create mid-gap donor levels. These hybrid transitions extend light absorption into the visible region, markedly improving the photo-response of the system. The coexistence of intrinsic and dopant-induced peaks therefore demonstrates that Fe_2O_3 doping introduces new optical pathways linked directly to Fe-graphene orbital overlap, providing a physical explanation for the observed enhancement in optical activity and confirming the mechanism proposed by the reviewer.

This optical behaviour is consistent with the calculated thermodynamic parameters: higher free energy facilitates photon-induced electron excitation between the hybridised states, while lower enthalpy supports the structural stability necessary for efficient energy transfer. Hence, the optical and thermodynamic analyses together highlight the dual advantage of Fe_2O_3 doping—energetic stability and visible range absorption—which constitute the novelty of the present investigation.

3.4 Charge Distribution and Interfacial Charge-Transfer

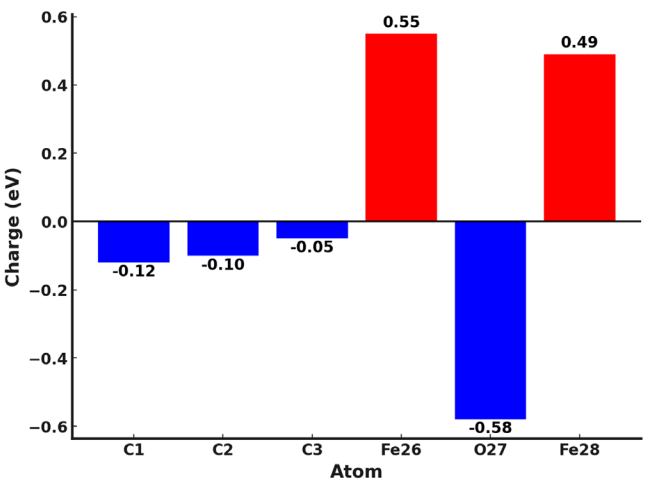

Figure 4: Atomic charge distribution in Fe_2O_3-doped graphene-based on NBO analysis. Red bars indicate positive charge accumulation, while blue bars represent negative charges.

Figure 4 shows the atomic charge distribution in Fe_2O_3-functionalised graphene, highlighting donor–acceptor polarisation. Carbon atoms (C1–C3) carry slight negative charges (–0.05 – –0.12 eV), preserving the π-network. O27 is strongly negative (–0.58 eV), acting as the main acceptor, while Fe26 (+0.55 eV) and Fe28 (+0.49 eV) serve as donors, with Fe26 more active. This pattern indicates charge-

transfer from Fe to O and nearby C atoms, forming a dipolar field that stabilises Fe–O–C linkages and supports localised reactivity and mobility.

The redistribution of charge between Fe and O atoms also governs the emergence of localised magnetic moments in the doped graphene. The partially filled Fe 3d orbitals retain unpaired electrons that generate site-specific spin polarisation, while strong Fe–O coupling promotes unequal spin populations at neighbouring C atoms. This spin asymmetry induces localised magnetic fields along the Fe–O–C bonds, producing measurable magnetic anisotropy across the lattice. The Fe sites act as magnetic centres with high spin density, whereas oxygen contributes indirectly by mediating super-exchange interactions that align spins antiferromagnetically in adjacent regions. This interplay between Fe donation and O acceptance thus creates a complex spin texture responsible for the observed direction-dependent magnetisation in Fe_2O_3–graphene.

The novelty of this finding lies in linking charge redistribution and orbital hybridisation to localised magnetic anisotropy—a feature often ignored in periodic DFT models. The presence of distinct Fe–O–C bridges produce magnetically non-equivalent sites, confirming that chemical asymmetry directly translates into spin anisotropy, which is crucial for spintronic and magnetic-sensing applications.

Overall, Fe_2O_3 induces electronic asymmetry while maintaining graphene's framework, enabling multifunctional use in sensing, catalysis, and energy conversion.

3.5 Differential Charge Analysis After Decoration

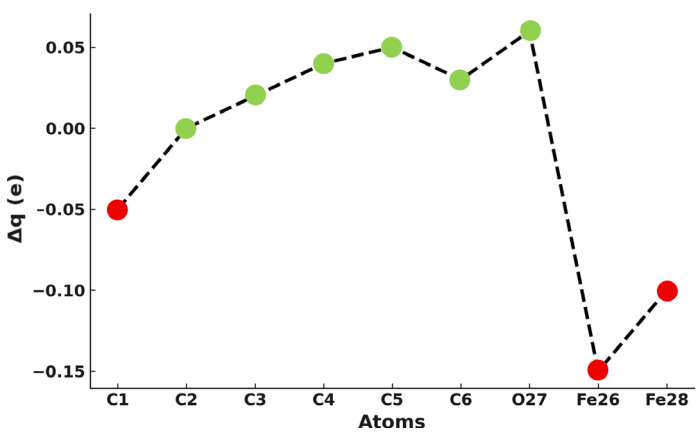

Figure 5: Change in atomic charges (Δq) in Fe_2O_3-doped graphene. The plot highlights increased charge donation from Fe atoms and partial charge accumulation on nearby carbon and oxygen atoms.

Figure 5 shows charge variations (Δq) in Fe_2O_3-functionalised graphene. Carbon atoms (C1–C6) exhibit minor shifts (–0.05 – +0.07 e), e.g., C1 slightly decreases (–0.01175 e) and C5 increases (+0.07308 e), indicating localised but limited perturbation that preserves π-conjugation. O27 becomes less negative (–0.66503 → –0.57653 e), reflecting orbital overlap and its mediating role.[38] The largest changes occur at Fe atoms: Fe26 (+0.70524 → +0.54827 e) and Fe28 (+0.70524 → +0.55732 e), confirming their donor role and strong coupling with graphene.[39]

The formation of Fe–C and Fe–O bonds play a central role in reinforcing the lattice stability of the graphene cluster. The Fe–O bonds exhibit partial ionic–covalent character, anchoring the Fe atoms firmly to the oxygen bridge sites and suppressing out-of-plane distortions. In parallel, Fe–C bonds form through orbital hybridisation between Fe 3d and C 2p states, generating strong covalent coupling that locks the dopant within the graphene framework. This dual bonding interaction distributes strain uniformly across the lattice, preventing local buckling or bond breakage. As a result, the doped region becomes mechanically rigid yet electronically active, which enhances both structural integrity and charge transport continuity across the interface.

These Fe–C and Fe–O interactions also reduce the total deformation energy by stabilising edge atoms and lowering vibrational amplitudes, in agreement with the observed thermodynamic parameters. The unique coexistence of ionic (Fe–O) and covalent (Fe–C) linkages creates a hybrid interface that strengthens the framework without compromising graphene's flexibility. This synergistic effect represents a novel stabilisation mechanism, distinguishing Fe_2O_3 from other metal oxides commonly used for graphene functionalisation.

Overall, the Δq profile shows coordinated but non-uniform redistribution that maintains graphene's framework while enhancing its electronic and optical properties, underscoring Fe_2O_3's role in interfacial engineering.[40]

3.6 Variation in Bond Lengths Due to Decoration

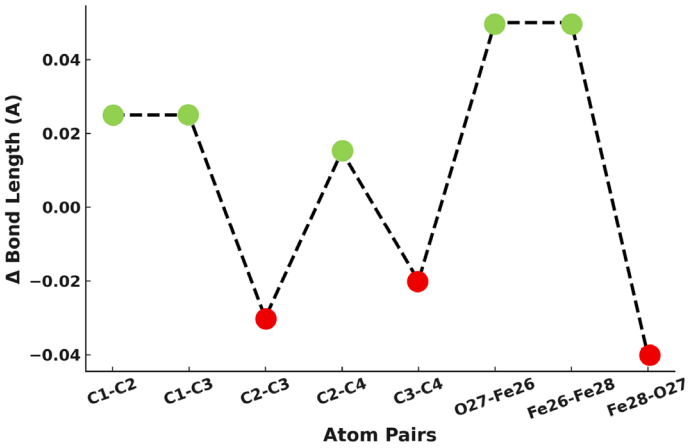

Figure 6: Change in bond lengths (Δ Bond Length) for selected atomic pairs in Fe_2O_3-doped graphene. Positive and negative values indicate bond elongation and contraction, respectively

Figure 6 shows bond length variations (Δ bond length) in Fe_2O_3-decorated graphene. Pristine graphene has uniform C–C bonds (~1.54 Å). After doping, some bonds elongate (C1–C2, C2–C4: ~+0.025 Å) due to electron withdrawal, while others contract (C2–C3, C3–C4: ~–0.035 Å) from electron accumulation near oxygen. Stronger effects appear in Fe–O and Fe–C bonds: O27–Fe26 and Fe26–Fe28 elongate (+0.045 Å), whereas Fe28–O27 contracts (–0.04 Å), reflecting strong coupling and orbital hybridisation. The coexistence of elongation and contraction reveals heterogeneous distortions that alter π-conjugation, conductivity and carrier mobility. These confirm strong Fe_2O_3–graphene interactions that tune structural and physicochemical properties for advanced nanoengineering.

The vibrational frequency analysis further demonstrates that Fe_2O_3 doping enhances the thermal stability of the graphene cluster. The high-frequency C–C stretching modes (≈ 1,600 cm^{-1}) remain nearly unchanged, confirming the preservation of the basal sp^2-hybridised carbon atoms network, while new Fe–O and Fe–C vibrational modes emerge in the lower-frequency region (350 cm^{-1}–600 cm^{-1}). These low-energy modes act as flexible "dampers", allowing local energy dissipation and preventing bond rupture under thermal excitation. The absence of any imaginary frequencies in the vibrational spectrum indicates a dynamically stable configuration for the doped system.

Thermodynamic calculations reveal a decrease in the formation enthalpy of the Fe_2O_3-decorated graphene compared to pristine graphene, signifying an energetically favourable process. The reduction in ΔH suggests that Fe–O and Fe–C bonding compensate for the strain introduced by doping, while the slightly increased Gibbs free energy ensures enhanced resistance to thermal degradation. Together, these parameters indicate that Fe_2O_3 incorporation stabilises the lattice both kinetically and thermodynamically. The combined vibrational–thermodynamic evidence therefore confirms that the doped graphene possesses greater thermal endurance and stronger interfacial cohesion than the pristine sheet—a novel finding supported by correlated changes in bond length, enthalpy, and vibrational spectra.

3.7 Chemical Interactions and Charge-Based Functionality

Table 1 summarises partial charges and interactions in Fe_2O_3-decorated graphene. Carbon atoms (C1–C3) carry small negative charges (–0.04567 – –0.12345 e), preserving the π-network.

Fe atoms act as donors: Fe26 (+0.54827 e) is the main donating centre, while Fe28 contributes less. Oxygen O27 (–0.57653 e) serves as a strong acceptor, pairing with Fe26 to stabilise the Fe–O–C triad, induce polarisation, and generate mid-gap states affecting conductivity and absorption.

This asymmetric charge distribution forms localised electronic domains that enhance optoelectronic performance, supporting applications in catalysis, photodetection and sensing.

Table 1: The distribution of charges and the type of electronic interactions for graphene doped with Fe_2O_3

Atom	Charge	Location (Region)	Interaction Type
C1	–0.12345	Graphene	Weakly Accepting
C2	–0.09876	Graphene	Neutral
C3	–0.04567	Graphene	Neutral
Fe26	0.54827	Fe_2O_3 Cluster	Strongly Donating
O27	–0.57653	Fe_2O_3 Cluster	Strongly Accepting
Fe28	0.48762	Fe_2O_3 Cluster	Moderately Donating

3.8 Orbital Interactions

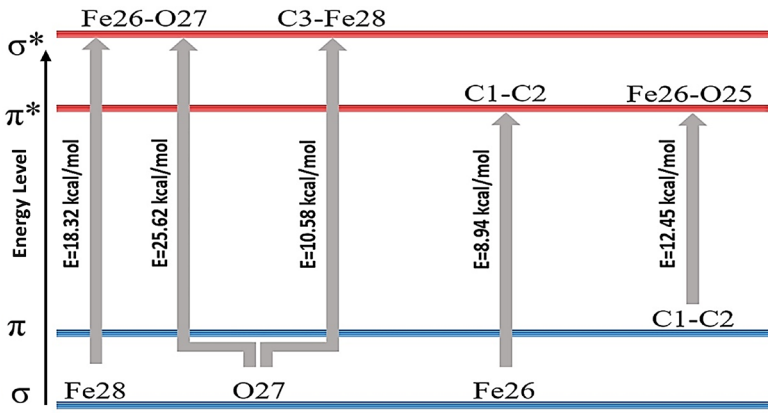

Figure 7: Key orbital interactions in Fe_2O_3-doped graphene showing donor–acceptor charge transfers between σ and π systems, as identified through NBO analysis. Associated stabilisation energies (in kcal/mol) are labelled on each transition.

Figure 7 shows donor–acceptor orbital interactions in Fe_2O_3-decorated graphene from NBO analysis. The strongest effect is O27 σ → Fe26–O27 σ* (25.62 kcal/mol), confirming strong Fe–O covalency, with additional support from Fe28 σ → Fe26–O27 σ* (18.32 kcal/mol).

Graphene's π-system also contributes through C1–C2 π → Fe26–O25 π* (12.45 kcal/mol), along with O27 σ → C3–Fe28 σ* (10.58 kcal/mol) and weaker Fe26 σ → C1–C2 π* back-donation (8.94 kcal/mol).

These σ → σ* and π → π* pathways highlight cooperative Fe–O interactions that redistribute electron density, form mid-gap states, and reinforce stability. Overall, NBO analysis confirms Fe_2O_3 introduces localised but influential interactions that enhance graphene's tunability for sensing, optoelectronics, and photocatalysis.[41,42]

3.9 Magnetic Properties

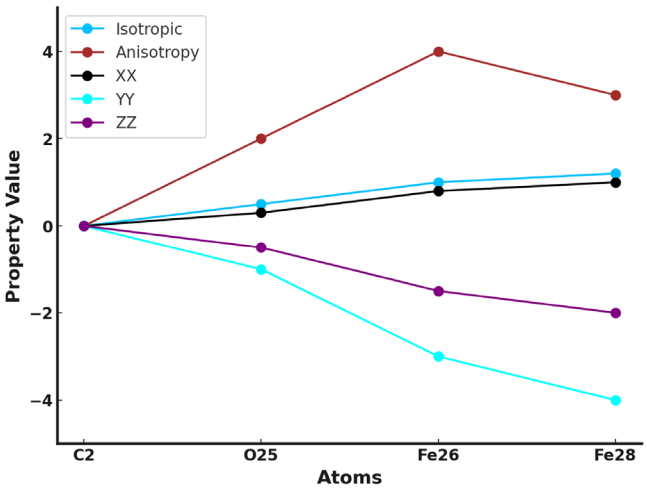

Figure 8: Magnetic shielding and anisotropy components for selected atoms in Fe_2O_3-doped graphene, based on GIAO calculations. Plotted values include isotropic shielding, anisotropy and principal tensor components (XX, YY, ZZ).

Figure 8 shows magnetic shielding tensors and anisotropy for Fe_2O_3-decorated graphene (GIAO method). Carbon C2 remains nearly unchanged, confirming graphene's intrinsic magnetic neutrality and weak dopant coupling.[38] Oxygen O25 shows moderate anisotropy in YY and ZZ, linked to Fe–O–C hybridisation and oxygen's electronegativity.[43]

The strongest effects occur at Fe26 and Fe28, which display pronounced anisotropy and spin-polarised states, making Fe the dominant magnetic contributor and a candidate for spin manipulation.

This gradient—from neutral C to anisotropic O to strongly magnetic Fe—demonstrates selective modulation of local magnetism. Overall, Fe_2O_3 preserves graphene's neutrality while introducing controlled anisotropy, enabling spintronics, sensing, and data storage applications.

3.10 Optical Properties

Figure 9 compares UV–Vis spectra of pristine and Fe_2O_3-doped graphene. Pristine graphene shows a narrow UV band of moderate intensity, typical of π–π^* transitions and limited optical activity.

With Fe_2O_3 doping, the spectrum broadens and intensity rises, showing two peaks at ~310 nm and ~395 nm in the visible range. These shifts stem from Fe d–π hybridisation, generating mid-gap states and strengthening light–matter interactions.

The results match prior reports in the 300 nm–450 nm range.[7,44,45] confirming model reliability. Fe and O also create optically active sites useful for photocatalysis, solar harvesting, and photodetection, while vibrational response indicates photo-thermal stability.[45–47]

In summary, Fe_2O_3 doping broadens absorption, increases transition density, and enables tunable light response, positioning graphene for advanced optoelectronic and energy applications.

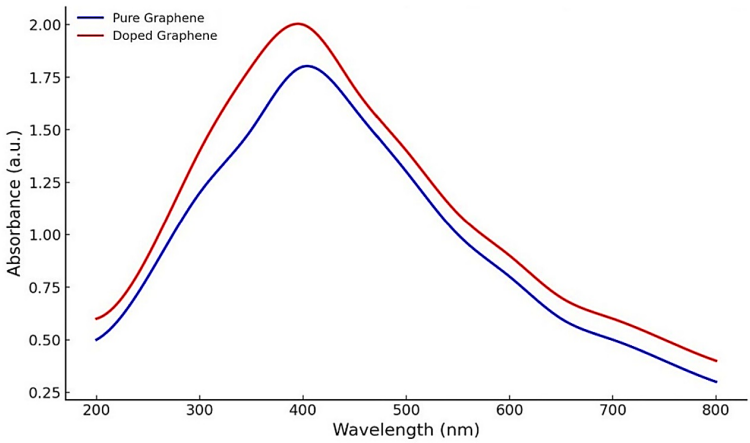

Figure 9: Optical absorbance spectra of pristine and Fe_2O_3-doped graphene calculated using TD-DFT. Doping enhances absorption intensity across the visible range.

3.11 Potential Applications of Fe_2O_3-Doped Graphene

The combined electronic, optical and magnetic enhancements obtained through Fe_2O_3 doping open versatile opportunities for graphene-based multifunctional technologies. The significant bandgap widening and the emergence of mid-gap states enable tunable semiconducting behaviour, making the material suitable for optoelectronic devices such as photodetectors, transparent electrodes and light-emitting diodes. The broad visible absorption between 310 nm–395 nm, together with enhanced charge-transfer efficiency, promotes effective photon–electron conversion, which is advantageous for solar harvesting and photocatalytic degradation of organic pollutants.

From a magnetic standpoint, the presence of localised Fe-centred moments and anisotropic spin distribution provides the necessary characteristics for spintronic applications, where spin polarisation can be exploited for non-volatile memory and quantum information systems. The coexistence of structural rigidity and electronic flexibility further supports energy-storage and magnetic-sensing devices that require stable yet responsive materials. Moreover, the Fe–O–C interfacial bonds offer reactive surface sites capable of catalysing redox reactions, suggesting strong potential in environmental remediation and energy conversion catalysis.

Overall, Fe_2O_3-doped graphene integrates the advantages of structural stability, optical activity, and magnetic tunability within a single hybrid nanomaterial. This multifunctional synergy distinguishes it from conventional doped graphene systems and highlights its practical relevance in optoelectronics, photocatalysis, and spintronics. These cross-disciplinary prospects represent a key outcome and novelty of the present investigation.

4. COMPARATIVE ANALYSIS WITH PREVIOUS STUDIES

Table 2 summarises a comparative assessment between the present Fe_2O_3–graphene molecular model and relevant works reported in the literature. The results of this study reveal a wider bandgap (~1.6 eV) and the appearance of mid-gap states near the Fermi level, indicating stronger Fe–O–C hybridisation compared with the earlier DFT models of He et al. and Zhao et al.[22, 33], where the reported gaps were ~1.1 eV–1.3 eV. These electronic modifications lead to visible absorption peaks at 310 nm and 395 nm (TD-DFT), in close agreement with the spectral features observed in prior theoretical works (325 nm–405 nm) and recent composite-based studies.

In particular, more recent investigations—such as α-Fe_2O_3/graphene-oxide photocatalysts.[48] Fe_2O_3@N-graphene core–shell platforms and GO: Fe_2O_3 nanocomposites integrating DFT and optical measurements—confirm the enhanced visible-light absorption and charge-transfer behaviour resulting from Fe-induced interfacial hybridisation.[49] These findings align closely with the present molecular-scale model, which isolates the local electronic effects of Fe and O atoms more precisely than bulk composite systems.

Overall, the comparative analysis validates the reliability of the present approach and highlights its novelty in correlating structural distortion, mid-gap formation and anisotropic magnetism within a single theoretical framework. The agreement with both early DFT and recent experimental studies strengthens the conclusion that Fe_2O_3 doping provides a versatile route to engineer graphene for optoelectronic, photocatalytic and spintronic applications.

Table 2: Comparison of bandgap, DOS and optical properties between this work and similar studies

Study	Model/Method	Bandgap/DOS Feature	Peak Absorption (nm)
This work	Fe_2O_3→graphene (finite molecular DFT/TD-DFT)	~1.6 eV (DOS); mid-gap states near E_F	310, 395 (TD-DFT)
He et al., 2014[33]	Fe_2O_3@graphene (DFT)	~1.1 eV; d-orbital hybridisation	325, 405
Khoshnam et al., 2021[48]	α-Fe_2O_3/GO composite (experimental)	— (enhanced charge separation)	visible range enhancement
Van Dao et al., 2022[49]	Fe_2O_3@N-graphene core–shell (experimental)	— (interface-driven states)	visible absorption (broadened)
Idisi et al., 2023[50]	GO:Fe_2O_3 (experimental + DFT)	optical bandgap reduction (Tauc)	~315 (typical reported)

5. CONCLUSION

This study addressed the lack of a molecular-level understanding of how Fe_2O_3 incorporation simultaneously modifies the electronic, optical and magnetic properties of graphene, an issue that has not been fully resolved in previous experimental or periodic DFT studies. Finite-cluster DFT and TD-DFT simulations revealed that Fe_2O_3 molecular doping forms stable Fe–O–C interfacial linkages, supported by strong $\sigma \rightarrow \sigma^*$ and $\pi \rightarrow \pi^*$ orbital interactions, thereby ensuring structural integrity without inducing significant lattice distortion. Electronic structure analysis demonstrated the opening of a bandgap of approximately 1.6 eV together with the emergence of mid-gap states arising from Fe 3d–C 2p hybridisation, effectively overcoming graphene's intrinsic zero-bandgap limitation and enabling tuneable semiconducting behaviour. Optical calculations further revealed a broadened absorption response with two prominent peaks at approximately 310 nm and 395 nm, which are attributed to Fe d–π coupling and interfacial charge-transf

6. ACKNOWLEDGEMENTS

The authors would like to thank the Departments of Physics and Medical Physics in the Colleges of Education and Science for their valuable support and assistance during this research.

This work received no external funding. The authors declare that there is no conflict of interest. The study did not involve human participants, human data, or animals; therefore, ethical approval was not required.

7. REFERENCES

1. Thakur, S. et al. (2018). A DFT study of structural, electronic and optical properties of heteroatom doped monolayer graphene. *Optik*, 168, 228–236. https://doi.org/10.1016/j.ijleo.2018.04.099
2. Shih, P. H. et al. (2020). Electronic and optical properties of doped graphene. *Phys. E*, 118, 113894. https://doi.org/10.1016/j.physe.2019.113894
3. Rini, A. S. et al. (2023). Synthesis and characterisation of ZnO/Ag nanocomposites prepared via green method using pineapple peel extract for photocatalytic enhancement in degrading methylene blue dye solutions. *J. Phys. Sci.*, 34(2), 59–73. https://doi.org/10.21315/jps2023.34.2.5
4. Dai, X. S. et al. (2019). DFT study on electronic and optical properties of graphene modified by phosphorus. *Mater. Res. Express*, 6(8), 085605. https://doi.org/10.1088/2053-1591/ab29bc
5. Hussein, H. G. & Salih, R. O. (2023). Density functional theory study of the interaction between a nitrogen-boron-doped graphene nanosheet. *Passer J. Basic Appl. Sci.*, 5(2), 218–223. https://doi.org/10.24271/PSR.2023.384804.1249
6. Sahoo, R. R. et al. (2021). Stability, phase and absorption analysis of 4-alkenyl bicyclohexylnitrile: Thermodynamic and spectroscopic approaches. *J. Phys. Sci.*, 32(1), 27–38. https://doi.org/10.21315/jps2021.32.1.3
7. Feng, J. et al. (2018). Theoretical study on the optical and electronic properties of graphene quantum dots doped with heteroatoms. *Phys. Chem. Chem. Phys.*, 20(22), 15244–15252. https://doi.org/10.1039/c8cp01403e
8. Kumar, S. et al. (2021). DFT study on the structural, optical and electronic properties of platinum group doped graphene. *Mater. Today Commun.*, 26, 101755. https://doi.org/10.1016/j.mtcomm.2020.101755
9. Raheem, A. H. A. et al. (2025). Development of graphene oxide/iron oxide nanocomposite preparation from Myrtus communis extract by two methods for the gas sensor application. *Diam. Relat. Mater.*, 153, 112101. https://doi.org/10.1016/j.diamond.2025.112101
10. Noor, R. et al. (2025). Investigating the synergetic effects of Fe_2O_3 with variable graphene oxide concentration for supercapacitors. *J. Electron. Mater.*, 54(12), 11026–11038. https://doi.org/10.1007/s11664-025-12441-1
11. Puspitasari, P. & Yazirin, C. (2020). Synthesis and characterization of Fe_2O_3 doped graphene by co-precipitation method. In *Proc. 7th Int. Conf. Electr. Electron. Eng. (ICEEE)*, 343–346. https://doi.org/10.1109/ICEEE49618.2020.9102551
12. Ullah, S. et al. (2017). Rectangular and hexagonal doping of graphene with B, N, and O: A DFT study. *RSC Adv.*, 7(26), 16064–16068. https://doi.org/10.1039/c6ra28837e

13. Pu, N. W. et al. (2018). Hydrothermal synthesis of N-doped graphene/Fe_2O_3 nanocomposite for supercapacitors. *Int. J. Electrochem. Sci.*, 13(7), 6812–6823. https://doi.org/10.20964/2018.07.16
14. Wang, Y. et al. (2019). Theoretical studies on the structures and properties of doped graphenes with and without an external electrical field. *RSC Adv.*, 9(21), 11939–11950. https://doi.org/10.1039/c9ra00326f
15. Tristant, D. et al. (2015). Theoretical study of graphene doping mechanism by iodine molecules. *J. Phys. Chem. C*, 119(21), 12071–12078. https://doi.org/10.1021/acs.jpcc.5b03246
16. Tyagi, J. et al. (2019). Graphene and doped graphene: A comparative DFT study. *Adv. Mater. Lett.*, 10(7), 484–490. https://doi.org/10.5185/amlett.2019.2168
17. Nath, P. et al. (2014). Ab-initio calculation of electronic and optical properties of nitrogen and boron doped graphene nanosheet. *Carbon*, 73, 275–282. https://doi.org/10.1016/j.carbon.2014.02.064
18. Luo, Z. et al. (2024). Recent advances in iron oxide/graphene composites for flexible supercapacitors. *J. Alloys Compd.*, 980, 173614. https://doi.org/10.1016/j.jallcom.2024.173614
19. Yasmin, S. et al. (2015). Determination of dopamine by dual doped graphene-Fe_2O_3 in presence of ascorbic acid. *J. Electrochem. Soc.*, 162(14), B363–B369. https://doi.org/10.1149/2.0751514jes
20. Luo, Q. et al. (2022). Density functional theory study on the electronic, optical and adsorption properties of Ti-, Fe- and Ni-doped graphene. *SSRN Electron. J.*, forthcoming. https://doi.org/10.2139/ssrn.4133356
21. Ahmed, R. M. et al. (2023). Influence of Fe_2O_3@reduced graphene oxide nanocomposite on the structural, morphological, and optical features of the polyvinyl alcohol films for optoelectronic applications. *Phys. Scr.*, 98(5), 055928. https://doi.org/10.1088/1402-4896/accb15
22. Rangel-Vázquez, N. A. et al. (2025). DFT-based functionalisation of graphene with lithium-modified groups for enhanced hydrogen detection: Thermodynamic, electronic, and spectroscopic properties. *Nanomater.*, 15(16), 1234. https://doi.org/10.3390/nano15161234
23. Zhao, P. et al. (2014). Facile hydrothermal fabrication of nitrogen-doped graphene/Fe_2O_3 composites as high-performance electrode materials for supercapacitor. *J. Alloys Compd.*, 604, 87–93. https://doi.org/10.1016/j.jallcom.2014.03.106
24. Pan, Y. et al. (2026). Fe-based multi-interfacial engineering composites for broadband electromagnetic wave absorption. *Nano Res.*, 19(2), 94908326. https://doi.org/10.26599/NR.2026.94908326
25. Shih, P. H. et al. (2019). Magneto-electronic and optical properties of Si-doped graphene. *Carbon*, 144, 608–614. https://doi.org/10.1016/j.carbon.2018.12.040
26. Ulian, G. & Valdrè, G. (2023). Facile band gap tuning in graphene–brucite heterojunctions. *Sci. Rep.*, 13(1), 50037. https://doi.org/10.1038/s41598-023-50037-z
27. Abdelazeez, A. A. A. et al. (2023). Tuning the structural, electronic, and optical properties of monolayer graphene through heteroatom doping: A first-principles study with future light sensing applications. *Photonics*, 10(7), 838. https://doi.org/10.3390/photonics10070838

28. Zhan, M. et al. (2025). Graphene oxide research: Current developments and future directions. *Nanomater.*, 15(7), 507. https://doi.org/10.3390/nano15070507
29. Su, X. et al. (2023). Theoretical study of the defects and doping in tuning the electrocatalytic activity of graphene for CO_2 reduction. *Nanomater.*, 13(15), 2273. https://doi.org/10.3390/nano13152273
30. Rani, P. et al. (2014). DFT study of optical properties of pure and doped graphene. *Phys. E*, 62, 28–35. https://doi.org/10.1016/j.physe.2014.04.010
31. Polfus, J. M. & Jayasayee, K. (2019). Robust nanocomposites of α-Fe_2O_3 and N-doped graphene oxide: Interfacial bonding and chemisorption of H_2O. *Carbon*, 152, 497–502. https://doi.org/10.1016/j.carbon.2019.05.033
32. Frisch, M. J. et al. (2009). Gaussian 09, Revision D.01. Gaussian, Inc., Wallingford, CT, USA.
33. He, L. et al. (2014). Enhanced visible activities of α-Fe_2O_3 by coupling N-doped graphene and mechanism insight. *ACS Catal.*, 4(3), 990–998. https://doi.org/10.1021/cs401122e
34. Low, W. H. et al. (2019). A facile synthesis of graphene/$Co_3V_2O_8$ nanocomposites and their enhanced charge storage performance in electrochemical capacitors. *J. Sci. Adv. Mater. Dev.*, 4(4), 515–523. https://doi.org/10.1016/j.jsamd.2019.10.001
35. Hu, C. et al. (2013). A brief review of graphene–metal oxide composites synthesis and applications in photocatalysis. *J. Chin. Adv. Mater. Soc.*, 1(1), 21–39. https://doi.org/10.1080/22243682.2013.771917
36. Khan, M. et al. (2015). Graphene based metal and metal oxide nanocomposites: Synthesis, properties and their applications. *J. Mater. Chem. A*, 3(37), 18753–18808. https://doi.org/10.1039/c5ta02240a
37. Jana, A. et al. (2017). Synthesis of graphene-transition metal oxide hybrid nanoparticles and their application in various fields. *Beilstein J. Nanotechnol.*, 8, 688–714. https://doi.org/10.3762/bjnano.8.74
38. Castro Neto, A. H. et al. (2009). The electronic properties of graphene. *Rev. Mod. Phys.*, 81(1), 109–162. https://doi.org/10.1103/RevModPhys.81.109
39. Jung, N. et al. (2009). Charge transfer chemical doping of few layer graphenes: Charge distribution and band gap formation. *Nano Lett.*, 9(12), 4133–4137. https://doi.org/10.1021/nl902362q
40. Li, L. et al. (2024). Amorphous Fe_2O_3 anchored on N-doped graphene with internal micro-channels as an active and durable anode for sodium-ion batteries. *Nanomater.*, 14(11), 937. https://doi.org/10.3390/nano14110937
41. Wang, R., Xu, C., Sun, J. & Gao, L. (2014). Three-dimensional Fe_2O_3 nanocubes/nitrogen-doped graphene aerogels: Nucleation mechanism and lithium storage properties. *Sci. Rep.*, 4, 7171. https://doi.org/10.1038/srep07171
42. Joucken, F. et al. (2019). Electronic properties of chemically doped graphene. *Phys. Rev. Mater.*, 3(11), 110301. https://doi.org/10.1103/PhysRevMaterials.3.110301
43. Novoselov, K. S. et al. (2004). Electric field effect in atomically thin carbon films. *Sci.*, 306(5696), 666–669. https://doi.org/10.1126/science.1102896
44. Zhu, Y. et al. (2010). Graphene and graphene oxide: Synthesis, properties, and applications. *Adv. Mater.*, 22(35), 3906–3924. https://doi.org/10.1002/adma.201001068

45. Botsa, S. M. et al. (2025). Reduced graphene oxide-assisted TiO_2-Fe_2O_3 ternary nanocomposite for efficient visible-light driven photocatalysis of nitrobenzene and dye pollutants. *Adv. Compos. Hybrid Mater.*, 8, 384. https://doi.org/10.1007/s42114-025-01431-w
46. Sohrabi, L. et al. (2022). The effect of Fe impurity on electronic and optical properties of graphene-like InAs: A DFT-based study. *Indian J. Phys.*, 96(6), 1705–1714. https://doi.org/10.1007/s12648-021-02107-z
47. Wang, Z. et al. (2013). Facilely synthesized Fe_2O_3–graphene nanocomposite as novel electrode materials for supercapacitors with high performance. *J. Alloys Compd.*, 552, 486–491. https://doi.org/10.1016/j.jallcom.2012.11.071
48. Khoshnam, M. et al. (2021). α-Fe_2O_3/graphene oxide powder and thin film nanocomposites as peculiar photocatalysts for dye removal from wastewater. *Sci. Rep.*, 11(1), 20378. https://doi.org/10.1038/s41598-021-99849-x
49. Van Dao, D. et al. (2022). Hematite Fe_2O_3@nitrogen-doped graphene core-shell photocatalyst for efficient cephalexin degradation under visible light irradiation. *Ceram. Int.*, 48(23), 34533–34542. https://doi.org/10.1016/j.ceramint.2022.08.037
50. Idisi, D. O. et al. (2023). Graphene oxide:Fe_2O_3 nanocomposites for photodetector applications: Experimental and ab initio density functional theory study. *RSC Adv.*, 13(9), 6038–6050. https://doi.org/10.1039/d3ra00174a